



© 2025. The Author(s). This is an open-access article distributed under the terms of the Creative Commons Attribution-ShareAlike 4.0 International Public License (CC BY SA 4.0, <https://creativecommons.org/licenses/by-sa/4.0/legalcode>), which permits use, distribution, and reproduction in any medium, provided that the article is properly cited.

# Adsorptive removal of sulfamethoxazole from water using carbon-mineral composites.

Piotr Słomkiewicz<sup>1\*</sup>, Beata Szczepanik<sup>1</sup>, Katarzyna Piekacz<sup>1</sup>,  
Klaudiusz Gołombek<sup>2</sup>, Maria Włodarczyk-Makuła<sup>3</sup>

<sup>1</sup>Jan Kochanowski University Kielce, Poland

<sup>2</sup>Materials Research Laboratory, Faculty of Mechanical Engineering, Silesian University of Technology, Poland

<sup>3</sup>Faculty of Infrastructure and Environment, Częstochowa University of Technology, Poland

\*Corresponding author's e-mail: [piotr.slomkiewicz@ujk.edu.pl](mailto:piotr.slomkiewicz@ujk.edu.pl)

**Keywords:** carbon-mineral composites, new adsorbents, antibiotic sulfamethoxazole removal

**Abstract:** The objective of this work was to synthesize new carbon-mineral composites and evaluate their ability to remove sulfamethoxazole from water. Carbon-halloysite (CHS1a,b, CHNT1a,b) and carbon-kaolinite (CKT1a,b) composites were prepared using fruit pomace waste as a carbon precursor. In addition, raw halloysite (HS), halloysite nanotubes (HNT), and kaolinite (KT) were used as templates in the carbonization process conducted under a nitrogen atmosphere at two temperature values: 500°C and 800°C. The morphology and structural characteristics of the obtained composites were investigated using SEM EDX, FT-IR, Raman spectroscopy, and low-temperature nitrogen adsorption methods. All the composites were mesoporous materials. SEM and FTIR results confirmed that the surfaces of HNT, HS, and KT were covered with carbon. The highest carbon content was observed in composites prepared with HNT, suggesting that the nanotube structure enhances carbon deposition. The adsorption of sulfamethoxazole on both the newly synthesized carbon-mineral composites and the unmodified minerals was also studied. The removal efficiency of sulfamethoxazole increased significantly for composites such as CHS1a, CHNT1a, and CKT1a obtained at 800°C, compared to the raw minerals. The optimal conditions for sulfamethoxazole removal, achieving a maximum efficiency of 84%, were found using CHS1a with a dosage of 6 g/dm<sup>3</sup> and an initial antibiotic concentration of 20 mg/dm<sup>3</sup>.

The adsorption kinetics of sulfamethoxazole on the most effective adsorbent, CHS1a, was described using the pseudo-second-order kinetic model and the multi-center Langmuir adsorption model. CHS1a composite can be considered a promising adsorbent for the removal of sulfamethoxazole from water.

## Introduction

The presence of antibiotics in water resources around the world is becoming an increasingly serious concern. Due to the extensive use and negative impacts on human health and environment, antibiotics are classified as "emerging contaminants" (Sagaseta de Ilurdoz et al. 2022, Jiang T. et al. 2024). Residual antibiotics can exert a bacteriostatic and bactericidal effects on microbial populations and contribute to the development of drug-resistant bacteria. The primary sources of antibiotics in aquatic environments include excretion, since approximately 50-80% of administered antibiotics are excreted without being metabolized, and the improper disposal of expired and unused medications. These substances subsequently enter sewage and wastewater treatment plants, which are not prepared to eliminate these waste compounds (Prasannamedha et al. 2019).

Sulfamethoxazole, a sulfonamide antibiotic, is commonly used to treat various bacterial infections, including pneumonia and infections of the urinary tract, ears, and intestines (Ma et al. 2020, Prasannamedha et al. 2019). Residues of sulfamethoxazole have been detected in both natural aquatic environment and aquaculture area (Parida et al. 2021, Chen et al. 2024, Zhang et al. 2016, Zhao et al. 2024). The concentrations of sulfonamides in these ecosystems range from ng/L to µg/L, and even at low exposure levels, they can have adverse effects on human health (Lu et al. 2020). Conventional wastewater treatment technologies are generally insufficient for removing antibiotics from water. As a result, advanced methods such as adsorption (Hu et al. 2022, Gamoń et al. 2022), multiphase photocatalysis (Biancullo et al. 2019), advanced oxidation processes (Wang et al. 2020), and microbial biodegradation (Kayal et al. 2022) are increasingly being explored. However, the large-scale implementation of biological or advanced

oxidation treatments is challenging due to the complexity of the processes and the high investment costs involved. Among these, adsorption is considered particularly promising because of its simple design and operation, high efficiency, and wide applicability (Hu et al. 2022, Balarak et al. 2021). A variety of adsorbents have been studied for the removal of antibiotics, including sulfamethoxazole. These include activated carbons, graphene, carbon nanotubes, biochars, zeolite, montmorillonite, and ion-exchange resins (Hu et al. 2022, Zhao et al. 2024).

Interest in using agricultural and forestry waste (biomass) as a source of biochar or activated carbon has been growing (Hu et al. 2022, Zhao et al. 2023, Tan et al. 2022). Biochar and activated carbons derived from sawdust, corn stalks, fruit stones and other lignocellulosic materials have been applied to antibiotics removal from water (Qalyoubi et al. 2024, Luo et al. 2018, Tang et al. 2018, Evers et al. 2022, Xiang et al. 2019). Pyrolysis (carbonization) processes can convert organic waste into carbon-based or carbon-mineral adsorbents (Leboda et al. 2005, Skubiszewska-Zięba et al. 2012). Clay minerals are also promising adsorbents due to their low cost, high availability, low toxicity, chemical and physical stability, and large specific surface area. However, unmodified mineral clays often show limited antibiotic removal efficiency. This is because antibiotics are structurally complex molecules with diverse functional groups, shapes, and molecular weights, distinguishing them from many other organic pollutants. Therefore, clay modification is often necessary to enhance their adsorption affinity toward antibiotics (Gülenay Hacıosmanoğlu et al. 2022). Combining clay minerals with carbon materials can significantly improve adsorption performance. Various clay-based composites have been developed, including montmorillonite (Anadao et al. 2014, Bakandritsos, et al. 2005), attapulgite (Chen et al. 2011), palygorskite (Wu et al. 2011, Wu et al. 2014, Wu et al. 2016), and halloysite (Wu et al. 2016, Jiang et al. 2014). These materials have been used for adsorption of phenolic compounds, dyes, and heavy metal cations from water.

Previously, we developed halloysite/carbon nanocomposites and used them as adsorbents for the removal of various pharmaceuticals: ketoprofen, diclofenac, naproxen, paracetamol,

chloroxylenol, and chlorophene from aqueous solutions. Saccharose, cellulose, and corrugated cardboard were used as carbon precursor, and the carbonization process was carried out under a nitrogen ( $N_2$ ) atmosphere (Szczepanik et al. 2019, Szczepanik et al. 2020, Szczepanik et al. 2023).

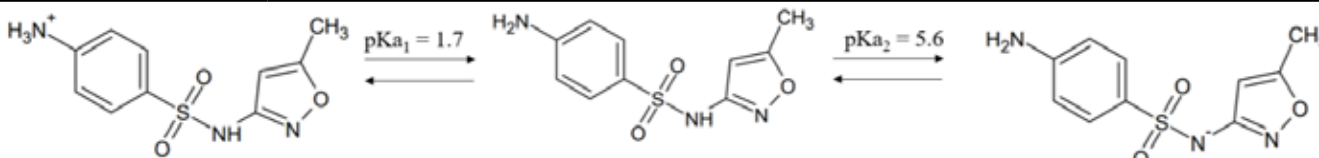
In this study, the new carbon-mineral adsorbents were synthesized using halloysite and kaolinite as templates, and fruit pomace (from apples, pears, and plums) as the carbon precursor. The composition and structural properties of the obtained composites were characterized using scanning electron microscopy (SEM), low-temperature nitrogen adsorption analysis, FTIR, and Raman spectroscopy. These results were compared with those of the unmodified clay minerals. The carbon-mineral composites, derived from readily available fruit waste and low-cost, environmentally friendly clay minerals, represent a new class of materials with potential applications in removing pollutants such as antibiotics from the natural environment. Sulfamethoxazole, a representative antibiotic, was selected as the adsorbate due to its poor affinity for clay minerals and strong interaction with carbonaceous materials. Therefore, this study aimed to determine whether carbon deposition on the surface of halloysite and kaolinite could enhance the removal efficiency of sulfamethoxazole from aqueous solutions. To the best of our knowledge, such carbon-clay composites have not previously been investigated as adsorbents for the removal of sulfamethoxazole from water.

## Experimental

### Materials and reagents

Sulfamethoxazole (purity > 99.0%) and natural kaolinite were purchased from Sigma-Aldrich. Raw halloysite (HS) was obtained from the "Dunino" strip mine in Legnica, Poland. Halloysite nanoclay (nanopowder) (HNT) was purchased from Merck KGaA, Darmstadt, Germany. Fruit pomace from Orchard Farm, Obrazów, Poland, was used as a raw material to prepare carbon-mineral adsorbents. Deionized water was used in all experiments. The physicochemical properties of sulfamethoxazole are presented in Table 1.

**Table 1.** Physicochemical properties of sulfamethoxazole

Compound	Sulfamethoxazole
	
IUPAC name	4-amino-N-(5-methyl-1,2-oxazol-3-yl) benzenesulfonamide
Chemical formula	$C_{10}H_{11}N_3O_3S$
Molecular size	12.26 Å
Molecular weight	253.28 g/mol
Water solubility	280 mg/dm <sup>3</sup> at 25°C
log $K_{ow}^*$	0.89

\* $K_{ow}$  – octanol - water partition coefficient

### Preparation of adsorbents

Mineral-carbon composites were obtained through a carbonization process using halloysite and kaolinite as carriers and fruit pomace as the carbon precursor. To prepare the composites, fruit waste was mixed with the appropriate mineral at a mass ratio 9:1 and heated under the nitrogen atmosphere from room temperature to either 500 °C or 800 °C (at a heating rate of 5 °C/min), then held at the final temperature for 1h in a muffle furnace. The resulting composites were designated as follows: CHS1a (mineral carrier: HS, mass ratio 9:1, temperature 800 °C), CHNT1a (mineral carrier: HNT, mass ratio 9:1, temperature 800 °C), CKT1a (mineral carrier: KT, mass ratio 9:1, temperature 800 °C), CHS1b (mineral carrier: HS, mass ratio 9:1, temperature 500 °C), CHNT1b (mineral carrier: HNT, mass ratio 9:1, temperature 500 °C), and CKT1b (mineral carrier: KT, mass ratio 9:1, temperature 500 °C). Fruit-vegetable pomace was also carbonized alone under the same conditions at 500 °C and 800 °C, and designated as P500 and P800, respectively.

### Characterization of adsorbents

The porous structure parameters of the obtained composites were determined using low-temperature nitrogen adsorption isotherms (−196 °C), measured with a volumetric adsorption analyzer (ASAP 2020, Micromeritics, Norcross, GA, USA). Detailed methodology is described in Szczepanik et al. (2023).

Scanning electron microscopy (SEM) images of the composites were acquired using a Zeiss Supra 35 microscopes equipped with an energy-dispersive X-ray (EDX) detector (Thermo Scientific™), operating at an accelerating voltage of 20 kV.

X-ray photoelectron spectroscopy (XPS) measurements of the purified halloysite and halloysite-carbon nanocomposites were carried out using a monoXPS system (SPECS, Berlin, Germany) at the Institute of Physics, Jan Kochanowski University, Kielce, Poland. Further experimental details are provided in Szczepanik et al. (2020).

FTIR spectra were recorded using a PerkinElmer Spectrum 400 FT-IR/FT-NIR spectrometer equipped with a Smart Endurance single-bounce diamond attenuated total reflectance (ATR) cell. Further details are provided in Szczepanik et al. (2023).

Raman spectra were recorded in the range of 2000–1500  $\text{cm}^{-1}$  using a Perkin-Elmer Raman Station 400 spectrometer equipped with a CCD detector and a diode laser (wavelength: 785 nm, power: 350 mW). For each sample, 5 scans were performed, with a scan time of 20 seconds. The spectral resolution was 1  $\text{cm}^{-1}$ .

Boehm's titration method was used to identify functional groups on the composites surface (Gamoń et al. 2022, Szczepanik et al. 2023). The pH value at the point of zero charge ( $\text{pH}_{\text{PZC}}$ ) for the obtained materials was determined by mass titration (Kodama and Sekiguchi 2006, Lim et al. 2013, Szczepanik et al. 2023).

### Adsorption method

Carbon-mineral composites and non-modified minerals were used as adsorbents for the removal of sulfamethoxazole. Kinetic and equilibrium adsorption were determined through batch experiments conducted at 25°C. All experiments were

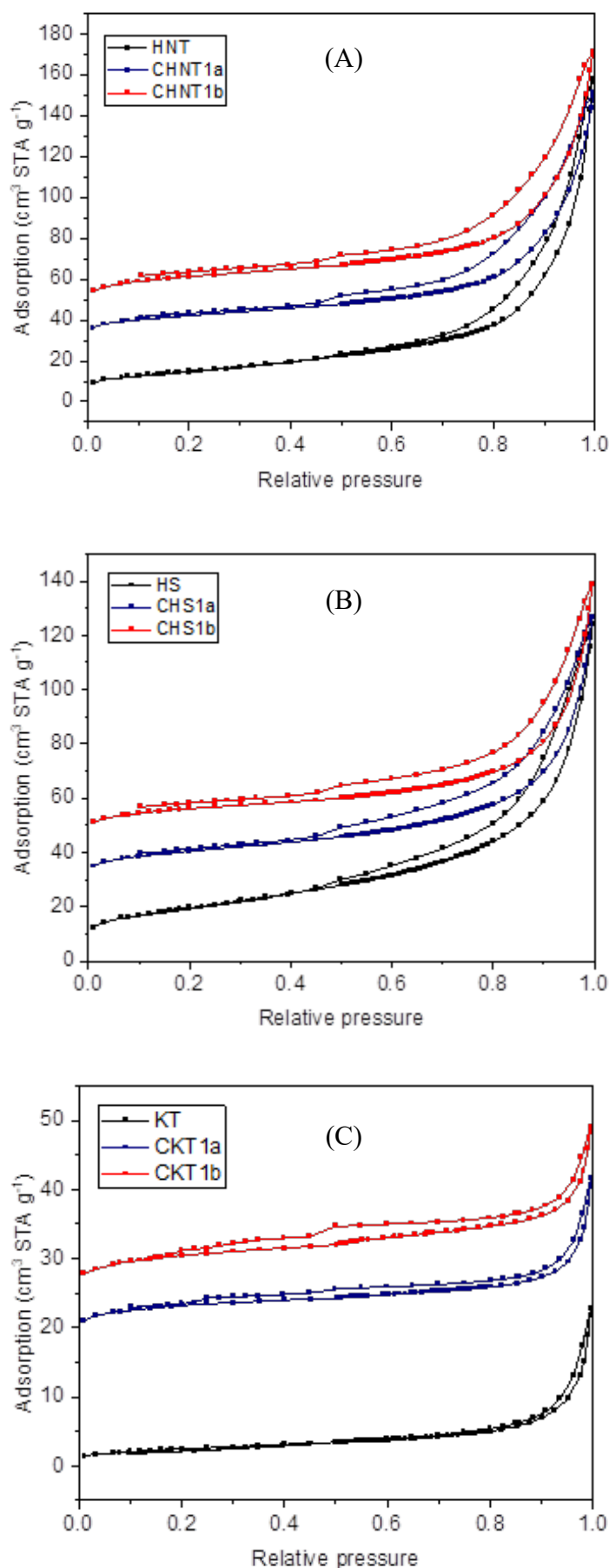


**Fig. 1.** Nitrogen adsorption–desorption isotherms for the HNT, CHNT1a, CHNT1b (A), the HS, CHS1a, CHS1b samples (B), and the KT, CKT1a, CKT1b samples (C).



performed in deionized water at approximately pH 6. The concentrations of the adsorbate solutions were determined using a spectrophotometric method (UV-Vis spectrophotometer Shimadzu UV-1800). The influence of the type and dose of adsorbent on the adsorption process was studied in conical flasks with a volume of 100 cm<sup>3</sup> (1000 cm<sup>3</sup> for kinetic studies). Between 0.05 g and 0.2 g of adsorbent was added to each flask, followed by 50 cm<sup>3</sup> of sulfamethoxazole solution at a concentration of 20 mg/dm<sup>3</sup>. The contents of each flask were

mixed for 24h with a stirring rate of 120 rpm. Measurements for kinetic studies were taken at 5, 10, 15, 30, 60, 90, 120, 180, 240, 300, 360, and 1440 minutes.

To obtain the adsorption isotherm, the concentrations of adsorbate solutions were 4, 8, 12, 16, and 20 mg/dm<sup>3</sup>. The adsorbent mass was 0.1 g, the contact time was 24 h, and the volume of adsorbate solution was 50 ml. Each flask was mixed at a stirring rate of 120 rpm for 24h),

After the defined contact period, the adsorbent was separated from the solution using a cup-type centrifuge. The resulting supernatant was then filtered through a filter with an average pore size of 0.1 mm. The absorbance of the adsorbate solution was measured at a wavelength of 261 nm.

The amount of adsorbate at equilibrium  $q_e$  and the percentage removal ( $R$ ) of the antibiotics by the adsorbent were calculated based on equations presented in (Szczepanik B. et al. 2023).

## Results and discussion

### Characterization of adsorbents

Nitrogen adsorption isotherms measured for halloysite, kaolinite, and their composites are presented in Figure 1. According to the IUPAC classification (Sing et al. 1985), the experimental isotherms for HS, HNT, and their composites correspond to type IV, confirming their mesoporous nature. The isotherms for kaolinite and its composites are also classified as type IV; however, the hysteresis loop is much narrower.

Structural parameters calculated from the adsorption isotherms are listed in Table 2. The specific surface areas  $S_{BET}$  of HS, HNT, and KT are 45.60 m<sup>2</sup>/g, 53.65 m<sup>2</sup>/g, and 8.93 m<sup>2</sup>/g, respectively. The  $S_{BET}$  values increase in the composites, especially for the carbon-kaolinite composites. The total pore volume  $V_t$  is comparable for HS and HNT but decreases in the halloysite-carbon composites. This value is significantly lower for KT compared to HS and HNT, but increases for the kaolinite-carbon composites. The mesoporosity values confirm that all studied materials are mesoporous in nature. The values of  $S_{BET}$  and  $V_t$  for P500 and P800 are low, at 0.90 m<sup>2</sup>/g, 6.26 m<sup>2</sup>/g, 0.0009 cm<sup>3</sup>/g, and 0.0044 cm<sup>3</sup>/g, respectively.

SEM images of the HNT, HS, KT samples, as well as the CHNT1a, CHS1a, CKT1a, CHNT1b, CHS1b, and CKT1b composites, along with their microscopic analysis including elemental composition obtained via EDS, are presented in Figs. 2-4. The CHNT1a sample (Fig. 2A) primarily consists of tubular particles covered by irregularly shaped particles. In the case of CHS1a (Fig. 2B), the number of tubular particles is lower, and larger irregular particles can be observed covering the halloysite. The CKT1a sample (Fig. 2C) differs from the others; its SEM image shows many flat kaolinite particles covering small fragments. The presence of carbon in all composites was confirmed by EDS analysis (Fig. 3). The carbon content decreases from 30.8% in CHNT1a and 27.2% in CHS1a (to 14.1% in CKT1a). SEM images of the CHNT1b and CHS1b samples resemble those of the corresponding halloysite composites obtained at 800°C, although the particles covering the halloysite appear larger. In the case of the kaolinite composites (CKT1a and CKT1b), the SEM images of the samples obtained at 800°C and 500°C are similar.

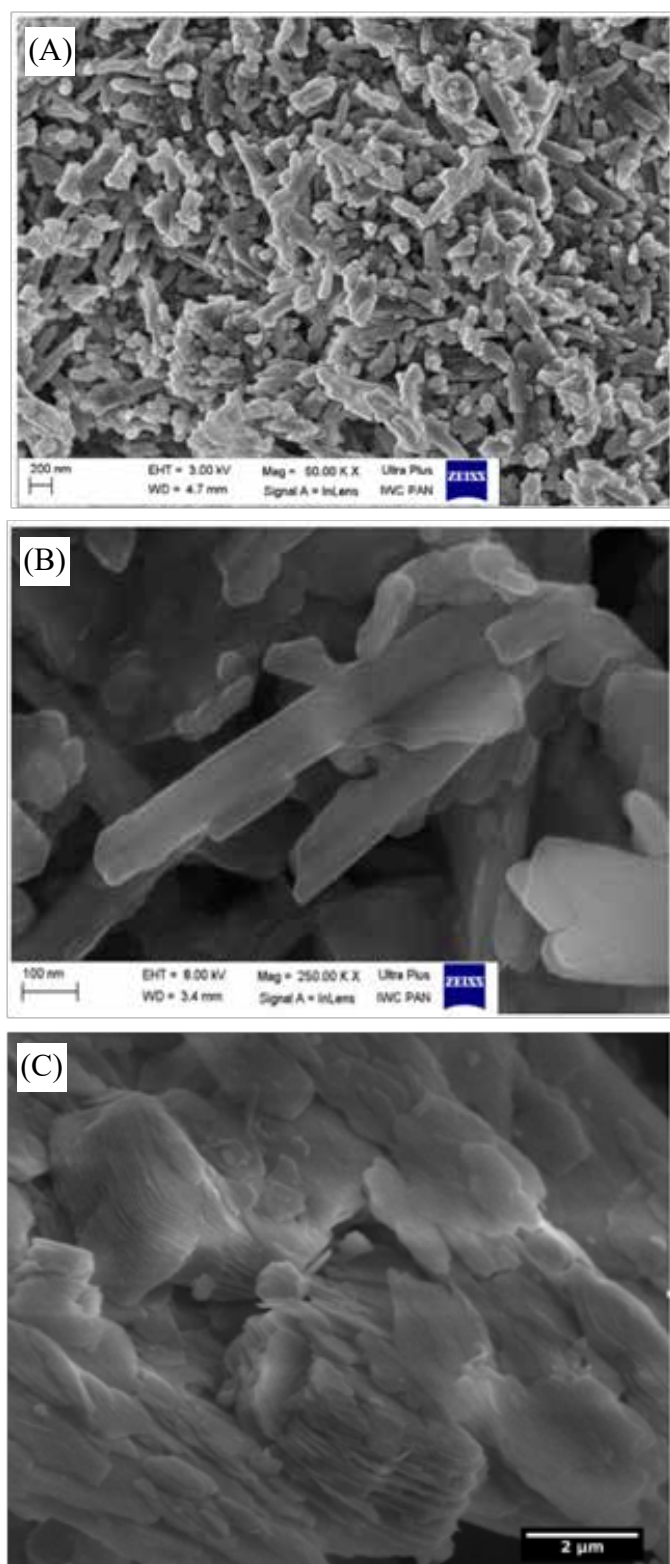


Fig. 2. SEM images of HNT (A), HS (B), and KT (C) samples.

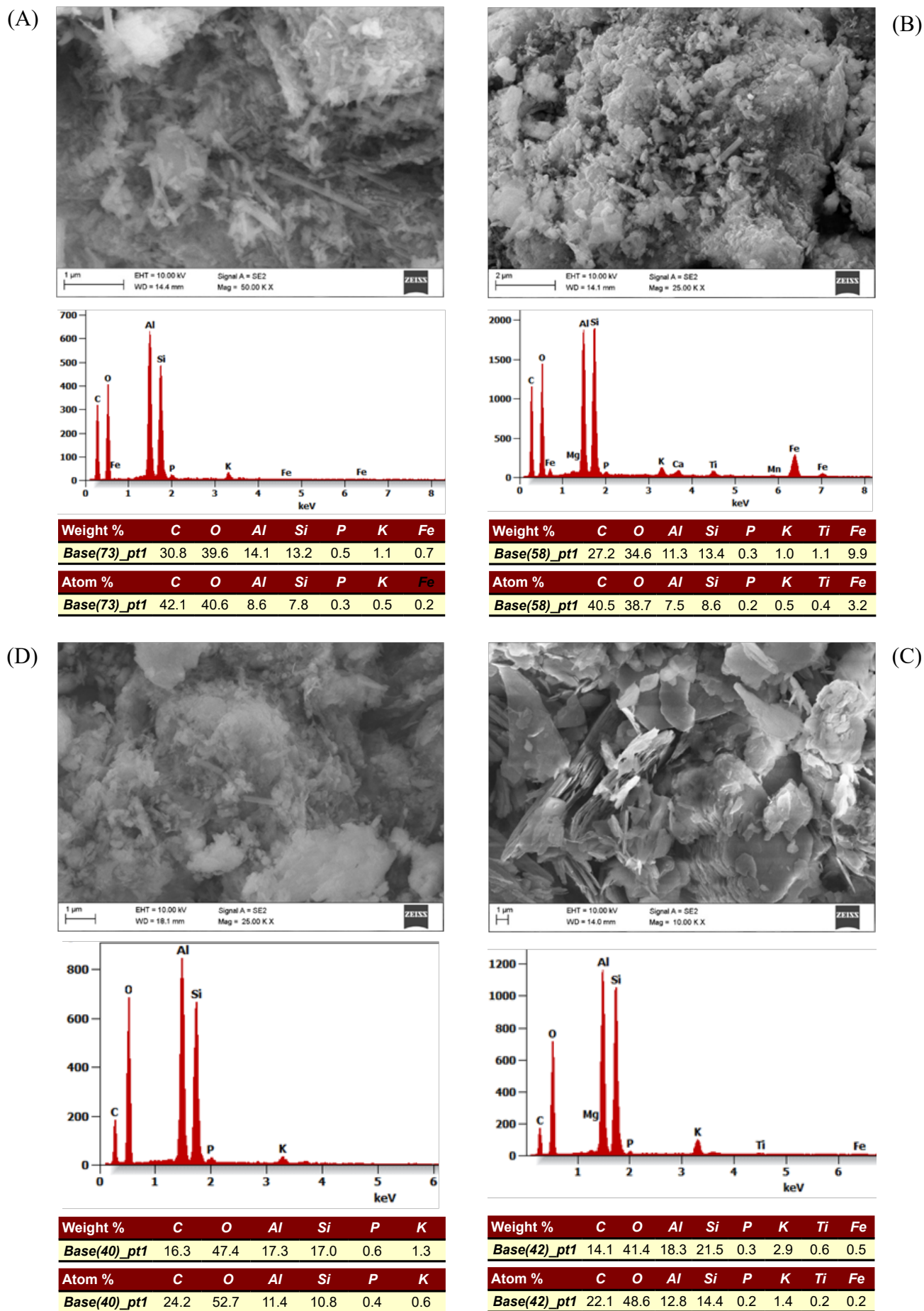


Fig. 3. SEM images of CHNT1a (A), CHS1a (B), and CKT1a (C) samples and their microscopic analysis including elemental composition with the EDS method.

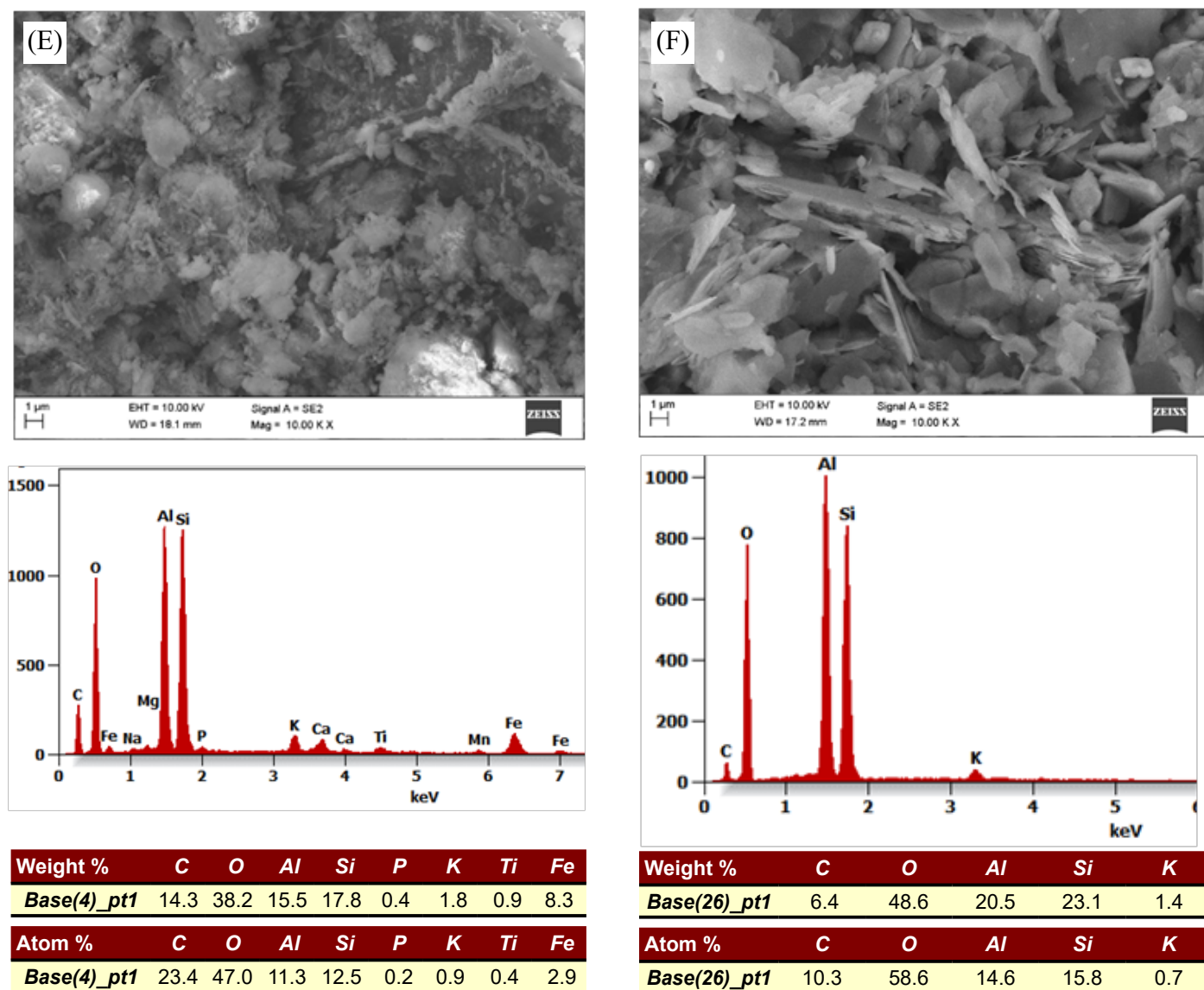
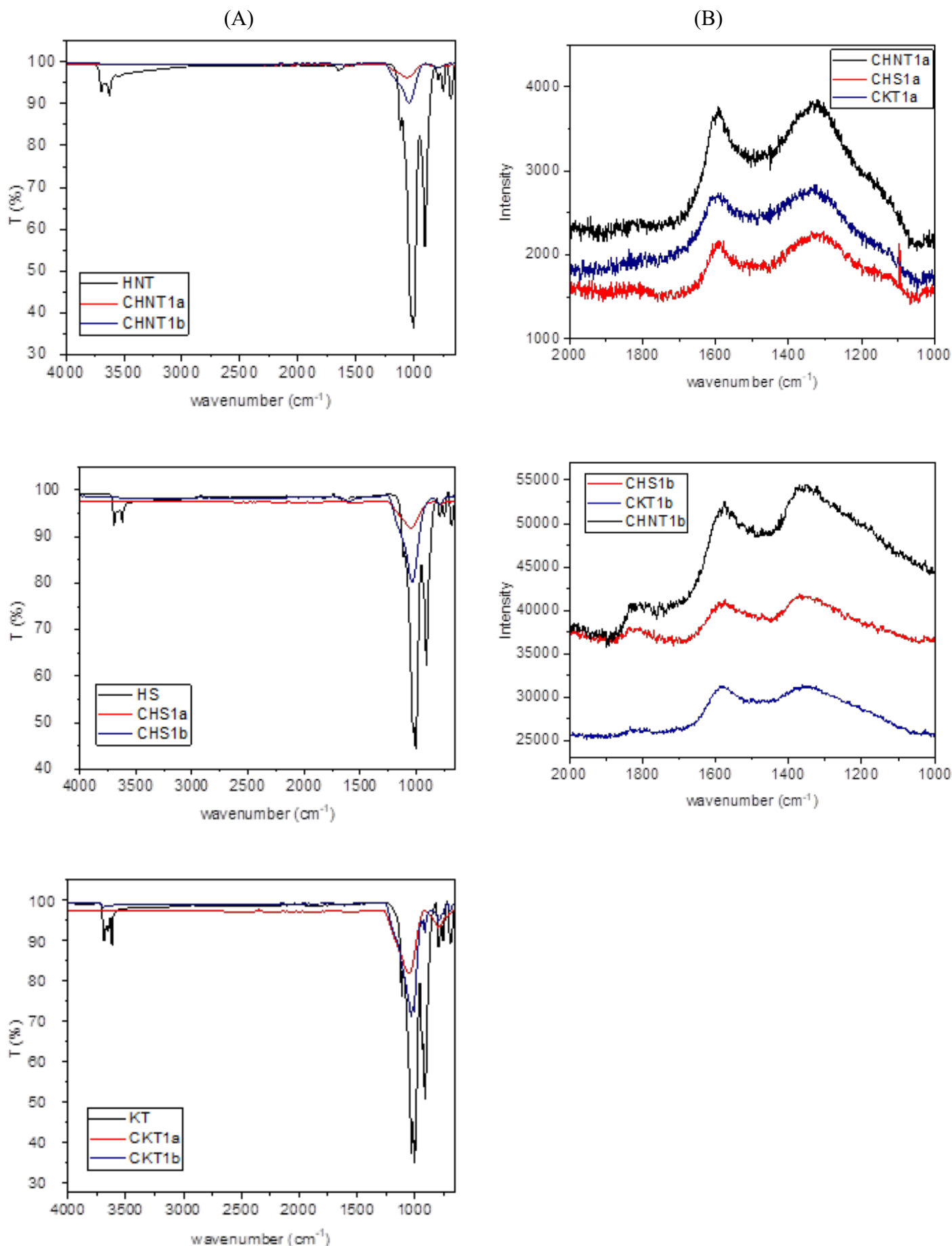


Fig. 4. SEM images of CHNT1b (D), CHS1b (E), CKT1b (F) samples and their microscopic analysis including elemental composition with the EDS method.

Table 2. Structural parameters of HS, HNT, KT and carbon-mineral composites

Composites	$S_{\text{BET}}$ $\text{m}^2/\text{g}$	$V_t$ $\text{cm}^3/\text{g}$	$V_{\text{mi}}$ $\text{cm}^3/\text{g}$	$V_{\text{me}}$ $\text{cm}^3/\text{g}$	Mesoporosity %
HS	45.60	0.1925	0.0019	0.1906	99
HNT	53.65	0.2202	0.0016	0.2186	99
KT	8.93	0.0294	-	0.0294	100
CHS1a	71.38	0.1534	0.0134	0.1400	91
CHNT1a	77.01	0.1908	0.0149	0.1759	92
CKT1a	45.02	0.0434	0.0140	0.0294	68
CHS1b	56.78	0.1393	0.0092	0.1301	93
CHNT1b	74.89	0.1882	0.0103	0.1779	95
CKT1b	36.42	0.0402	0.0078	0.0324	81
P500	0.90	0.0009	0.0005	0.0004	56
P800	6.26	0.0044	0.0036	0.0008	-



**Fig. 5.** (A) FTIR spectra of mineral samples (HNT, HS, and KT) and composites measured for the 650–4,000 cm<sup>-1</sup> region, (B) Raman spectra of mineral samples (HNT, HS, and KT) and composites.



XPS measurements were carried out for the CHNT1a and CHS1a samples. The conversion of carbon content from atomic percentage to weight percentage yielded carbon contents of 26 wt% for CHNT1a and 28 wt% for CHS1a in the carbon-halloysite composites.

FTIR spectra of the mineral samples (HNT, HS, and KT) and their corresponding composites (CHNT1a, CHNT1b, CHS1a, CHS1b, CKT1a, and CKT1b) are presented in Fig. 5A. The FT-IR spectra of the mineral samples show characteristic bands typical of kaolin-group minerals (Yuan et al. 2012, Joussein E. et al. 2007, Cheng H. et al. 2010). The bands in the range of 3,700–3,600 cm<sup>-1</sup>, corresponding to the O-H stretching vibrations in halloysite and kaolinite, are not observed in most composites, except for the sample CKT1b, where a significant reduction in intensity is visible. Additionally, the intensity of the bands in the range of 1,250–650 cm<sup>-1</sup> is greatly reduced, particularly in the composites obtained at 800°C. These changes indicate that the surfaces of HNT, HS, and KT are covered with carbon.

The mineral-carbon adsorbents were characterized using the Raman spectroscopy to obtain information about the structure of carbon deposits on the minerals. The Raman spectra (Fig. 5B) show two main peaks at ~1590 cm<sup>-1</sup> and ~1360 cm<sup>-1</sup>. The first peak can be assigned to the E<sub>2g</sub> mode (the G band “Graphite”) and the second one to the A<sub>1g</sub> mode (the D band, “Defect” or diamond-like structures) (Skubiszewska-Zięba et al. 2012).

The degree of carbon graphitization *R* was calculated using Equation (3), and the crystallinity of carbon was determined using Equation (4):

$$R = \frac{I_D}{I_G} \quad (3)$$

$$K = \left( \frac{I_G}{I_G + I_D} \right) \cdot 100\% \quad (4)$$

The values of the *R* parameter and the crystallinity coefficients for the mineral-carbon composites are presented in Table 3.

The results of the Boehm analysis for the composites showed the presence of carbonyl groups (0.375 mmol/) and basic functional groups (1.13 mmol/g). The number of basic groups was considerably higher than that of acidic groups on the surface of all composites. The point of zero change (*p*<sub>HPZC</sub>) of the HC-24 sample equaled 6.45 (Fig. 6).

### Adsorption experiments

The removal efficiency of sulfamethoxazole by halloysite, kaolinite, carbonized fruit-vegetable pomace, and mineral-carbon composites is shown in Figure 7. The minerals exhibit a similar, low degree of sulfamethoxazole removal from water, which is lower than 10%. A significant increase in removal efficiency is observed for the following composites: CHNT1a, CHS1a, and CKT1a, which were obtained at 800°C. Halloysite was used as the mineral support for these composites. In contrast, the carbonized pomace alone did not adsorb sulfamethoxazole.

### Effect of adsorbent dose

The dependence of the sulfamethoxazole removal efficiency on the adsorbent mass was examined for the composites with

**Table 3.** The values of the *R* parameter and crystallinity coefficients for the mineral-carbon composites

Adsorbent	Parameter <i>R</i>	Crystallinity coefficient <i>K</i> , %
CHNT1a	3.29	23.33
CHS1a	4.50	18.20
CKT1a	1.02	49.59
CHNT1b	2.64	27.45
CHS1b	3.15	24.09
CKT1b	4.79	17.28

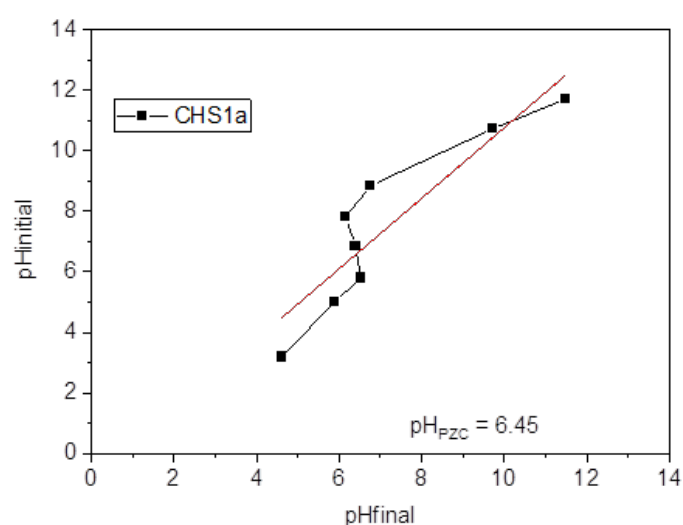


**Fig. 6.** Determination of *p*<sub>HPZC</sub> value on the CHS1a adsorbent.

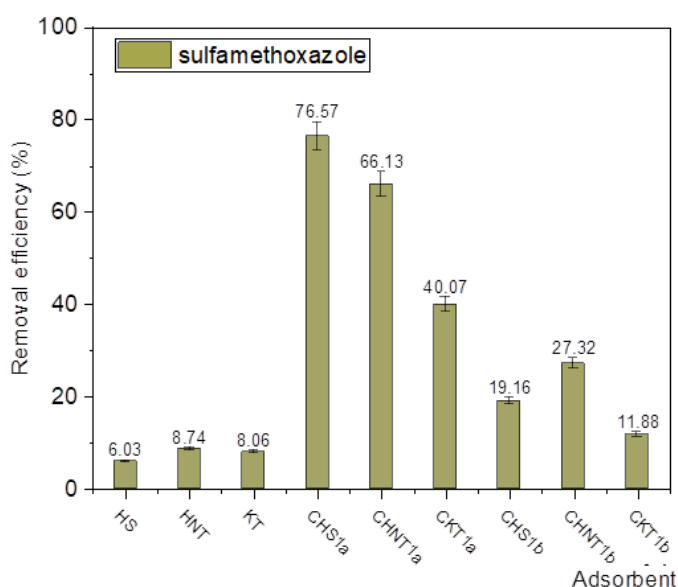


**Fig. 7.** Removal efficiency of sulfamethoxazole for clay minerals, carbonized fruit-vegetable pomace, and carbon-mineral adsorbents (adsorbent dose: 0.2 g, concentration of sulfamethoxazole solution: 20 mg/dm<sup>3</sup>, volume of antibiotic solution: 50 cm<sup>3</sup>, contact time: 24 h, and temperature: 25°C).



**Table 4.** Kinetic parameters of sulfamethoxazole adsorption on the C-HS1a adsorbent

Equation	Pseudo-first-order kinetic model	Pseudo-second-order kinetic model
	$q_t = q_e(1 - e^{-k_1 t})$	$q_t = \frac{q_e^2 k_2 t}{1 + k_2 q_e t}$
Rate constant	$k_1$ (min <sup>-1</sup> )	$k_2$ (g mg <sup>-1</sup> min <sup>-1</sup> )
	0.011	0.167
Adsorption volume at equilibrium $q_e$	4,7	5,9
Regression coefficient	0.9534	0.9989

$q_t$  – the number of adsorbate milligrams adsorbed per unit mass of adsorbent (mg·g<sup>-1</sup>) at time  $t$  (min),

$q_e$  – the number of adsorbate milligrams adsorbed per unit mass of adsorbent (mg·g<sup>-1</sup>) at equilibrium,

$k_1$  – rate constant pseudo-first-order kinetic model,

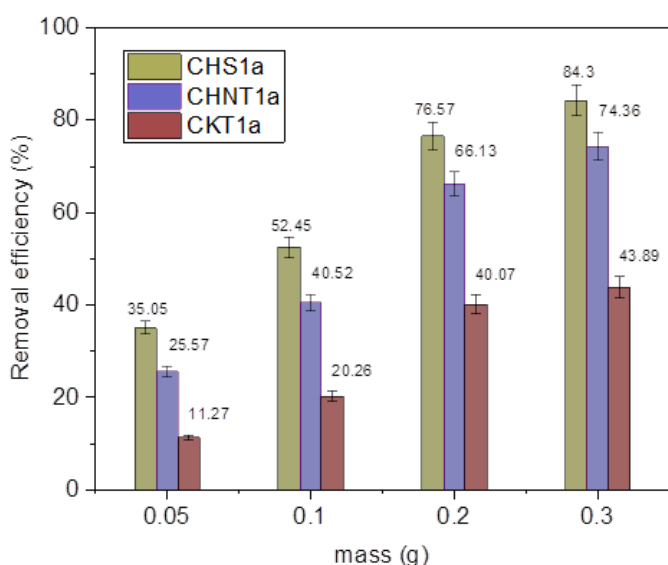
$k_2$  – rate constant pseudo-second-order kinetic model,

**Table 5.** Intra-particle diffusion model parameters

Equation	$q_t = k_d t^{1/2} + c$
$k_{d1}$ (mg g <sup>-1</sup> min <sup>-1/2</sup> )	0.75
$c_1$ (mg g <sup>-1</sup> )	0.47
Regression coefficient	0.8819
$k_{d2}$ (mg g <sup>-1</sup> min <sup>-1/2</sup> )	0.03
$c_2$ (mg g <sup>-1</sup> )	4.88
Regression coefficient	0.8757

$k_{id}$  – intra-particle diffusion rate constant (mg·g<sup>-1</sup>·min<sup>-1/2</sup>),

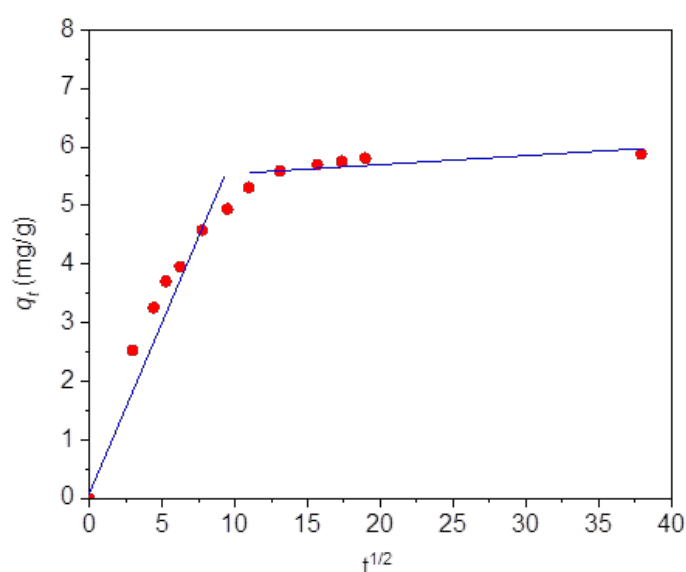
$c$  – intercept, which represents the thickness of the boundary layer (mg·g<sup>-1</sup>).

**Fig. 8.** Removal efficiency of sulfamethoxazole for carbon-mineral adsorbents (concentration of sulfamethoxazole solution: 20 mg/dm<sup>3</sup>, volume of antibiotic solution: 50 cm<sup>3</sup>, contact time: 24 h, and temperature: 25°C).

the highest adsorption capacities: CHNT1a, CHS1a, and CKT1a. Adsorbent doses ranging from 0.05 to 0.3 g were used. The sulfamethoxazole concentration was 20 mg/dm<sup>3</sup>, with a contact time of 24 h at a temperature of 25°C. The results are presented in Fig. 8. For all composites, the removal efficiency increased with increasing adsorbent mass. At each adsorbent dose, the efficiency followed the order CKT1a < CHNT1a < CHS1a, reaching a maximum value of 84.3% for 0.3 g of CHS1a).

### Kinetics

A comparison of the experimental data with three kinetic models - the pseudo-first-order, pseudo-second-order (Lagergren S. 1898, Ho Y.S. and McKay G. 1999), and the Weber-Morris diffusion model [49] - indicated that the pseudo-second-order kinetic model provided the best fit for sulfamethoxazole adsorption on the CHS1a adsorbent. The pseudo-first order and pseudo second-order rate constants ( $k_1$  and  $k_2$ ), along with

**Fig. 9.** The intra-particle diffusion of sulfamethoxazole on the C-HS1a adsorbent (adsorbent dose: 1 g, concentration of sulfamethoxazole solution: 20 mg/dm<sup>3</sup>, volume of antibiotic solution: 0,5 dm<sup>3</sup>)

**Table 6.** Freundlich, Langmuir, Langmuir (multi-center) and Temkin equations parameters for the adsorption of sulfamethoxazole on the CHS1a adsorbent

Equation	Freundlich <sup>a</sup>	Langmuir <sup>b</sup> one-center adsorption without dissociation	Langmuir <i>n</i> -center adsorption without dissociation <sup>b</sup>	Temkin
	$a_i = K_F c_i^{1/n}$	$a_i = q_m \frac{K_L c_i}{1 + K_L c_i}$	$a_i = q_m \frac{(K_{nL} c_i)^{1/n}}{(1 + K_{nL} c_i)^{1/n}}$	$a_i = B \ln(K_T c_i)$
Adsorption equilibrium constant <i>K</i>	0.511	ns	0.014	0.40
Error	$5.6 \times 10^{-4}$	ns	$7.1 \times 10^{-4}$	0.006
Coefficient <i>n</i>	1.66	ns	1.05	—
Error	$5.13 \times 10^{-4}$	ns	0,004	—
Adsorption capacity <i>q<sub>m</sub></i>	—	ns	5.8	—
Coefficient <i>B</i>	—	ns	—	2.61
Chi-Square minimization	$3.21 \times 10^{-4}$	ns	$4.92 \times 10^{-4}$	$3.91 \times 10^{-5}$
Regression coefficient	0.9594	ns	0.9993	0.9628

$a_i$  – the number of adsorbate milligrams adsorbed per unit mass of adsorbent ( $\text{mg} \cdot \text{g}^{-1}$ ),

$c_i$  – adsorbate concentration ( $\text{mg} \cdot \text{cm}^{-3}$ ),

<sup>a</sup>  $K_F$  – adsorption equilibrium constant ( $\text{mg} \cdot \text{g}^{-1}$ ) ( $\text{dm}^3 \cdot \text{mg}^{-1}$ )<sup>1/n</sup>,

<sup>b</sup>  $K_L$  – adsorption equilibrium constant ( $\text{cm}^3/\text{mg}$ ),

<sup>c</sup>  $K_{nL}$  – the Langmuir *n*-center adsorption isotherm constant ( $\text{dm}^3 \cdot \text{mg}^{-1}$ )<sup>1/n</sup>,

<sup>d</sup>  $K_T$  – the Temkin isotherm constant ( $\text{dm}^3/\text{mg}$ ),

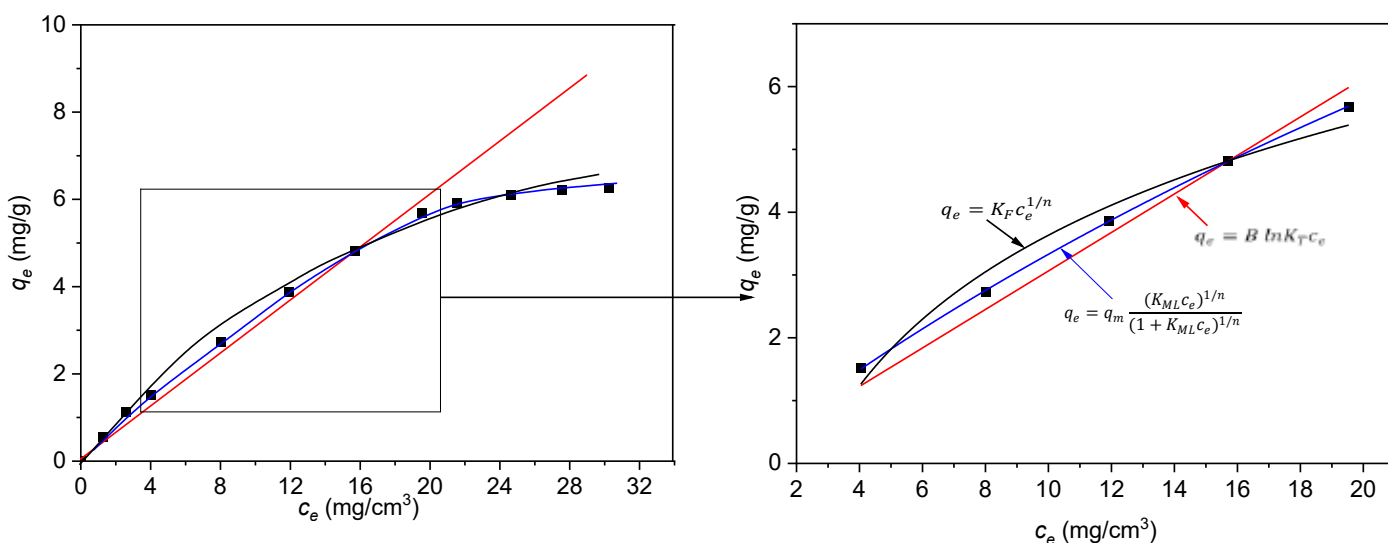
$q_m$  – adsorption capacity ( $\text{mg} \cdot \text{g}^{-1}$ ),

*B* – constant associated with the heat of adsorption,  $B = RT/b$ , *b* – the Temkin constant (J/mol), *T* – absolute temperature (K), *R* – gas constant.

the corresponding correlation coefficients ( $R^2$ ), are presented in Table 4. The kinetic parameters and adsorption isotherm simulations were calculated using the Levenberg–Marquardt least-squares method in the Origin Microcal software.

According to Weber and Morris model, the adsorption of sulfamethoxazole on the CHS1a adsorbent occurs in two stages. The first stage involves the external diffusion of adsorbate

molecules to the surface of the adsorbent, while the second stage corresponds to the gradual adsorption of sulfamethoxazole molecules, limited by intraparticle diffusion into the pores of the adsorbate [49]. The kinetic parameters of sulfamethoxazole adsorption on C-HS1a adsorbent, determined from the slopes and intercepts of the first and second linear part of graph (Fig. 9), are presented in Table 5.

**Fig. 10.** Calculation of adsorption equilibrium constant for sulfamethoxazole on the C-HS (9:1) adsorbent employing the experimental data (adsorbent dose: 0.1 g, volume of antibiotic solution: 50 cm<sup>3</sup>).

Fit of adsorption equilibrium equations (solid line) to the experimental data (points) by the Levenberg–Marquardt least-squares method.

**Table 7.** Comparison of the adsorption capacity of sulfamethoxazole on different adsorbents.

Adsorbent	Adsorption capacity $q_e$ (mg/g)	Reference
Montmorillonite	0.06	De Oliveira et al., 2018
Montmorillonite-carbon	0.63	Zhao and Zhou, 2019
Kaolinite	0.4	This study
Kaolinite-carbon	0.62	Zhao and Zhou, 2019
Kaolinite-carbon CKT1a	1.96	This study
Goethite-carbon	0.68	Zhao and Zhou, 2019
Zeolite	0.0025	Liu et al., 2020
Halloysite HS	0.3	This study
Halloysite-carbon CHS1a	5.8 mg/g	This study

### Adsorption isotherms and adsorption mechanism

Four adsorption isotherm models were used to analyze the sulfamethoxazole adsorption data: the (Freundlich model (Freundlich, 1906), the one-center and multi-center Langmuir models (Langmuir, 1916), and Temkin model (Temkin and Pyzhev, 1940). Nonlinear regression analysis was performed using the Levenberg–Marquardt least squares method in the OriginLab software).

As shown in Fig. 10, Freundlich and Temkin models do not fit the experimental data well. In the case of the Langmuir one-center model, there is no agreement between the experimental data and the isotherm equation. The best fit was obtained with the Langmuir multi-center adsorption model, with a correlation coefficient ( $R^2$ ) of 0.9993. This result confirms that adsorption occurs on multiple active sites on the adsorbent surface without dissociation of sulfamethoxazole molecules. The maximum adsorption capacity predicted by this model is 5.8 mg/g. All equation parameters, along with the correlation coefficients ( $R^2$ ) for sulfomethoxazole adsorption on the CHS1a adsorbent, are presented in Table 6.

The adsorption capacities of sulfamethoxazole on various mineral and mineral-carbon adsorbents reported in the literature are presented in Table 7. Although clays and other minerals are effective adsorbents for contaminants, their adsorption capacities for sulfamethoxazole are relatively low. However, modification of halloysite by carbon deposition significantly enhances its adsorption capacity.

The adsorption activity of composites containing carbon on the surface depends on the nature of the functional groups present on the surface, the textural properties of the adsorbent, and the properties of sulfomathoxazole. Sulfamethoxazole molecules exist in different forms depending on the pH: cationic below pH 1.7, neutral between pH 1.7 and 5.6, and anionic above pH 5.6 (Avisar D. et al, 2020). Since the adsorption experiments were carried out in aqueous solution at pH 6, the degree of dissociation, calculated using the Henderson–Hasselbalch equation, is approximately 30%. This indicates that the solution contains mainly neutral species and anions under these conditions.

The value of  $pH_{PZC}$  for the CHS1a adsorbent is 6.45. Therefore, at solution pH values below the  $pH_{PZC}$ , the total

surface charge is positive, while at higher pH values, the surface charge becomes negative due to the deprotonation of functional groups (Bernal V. et al. 2017). During the adsorption process, the solution pH is approximately 6, so the adsorbent surface is nearly neutral or slightly positively charged. Considering the good fit of the adsorption data to the PSO model and the chemical structure of sulfamethoxazole, the adsorption mechanism likely involves hydrogen bonding (Bandura et al., 2022, Terzyk 2001). The amine group in the sulfamethoxazole molecule can interact with oxygen-containing functional groups on the composite surface, such as carbonyl groups. The presence of different sulfamethoxazole forms and various functional groups on the adsorbent surface causes different adsorption interactions, which explains why the adsorption process follows the Langmuir adsorption model for multiple active centers.

### Conclusion

The use of adsorption technologies in wastewater treatment can reduce the concentration of antibiotics in the aqueous environment. Clay-based composites containing carbon derived from agricultural waste appears particularly promising for the removal of antibiotics such as sulfamethoxazole from water sources, due to their availability and ease of modification.

The adsorption capacity of clay minerals is closely related to their inherent properties, the type, size and shape of the contaminant molecules, as well as the operating conditions. Carbon-mineral adsorbents prepared using halloysite and kaolinite, with waste fruit pomace as carbon precursor, exhibited enhanced specific surface areas compared to unmodified minerals. All the resulting composites were mesoporous materials with carbon-coated surfaces.

The carbon content was higher in composites synthesized at 800°C compared to those obtained at 500°C. Additionally, composites prepared with kaolinite as a carrier contained less carbon compared to those obtained with halloysite (HS and HNT). The highest carbon content was observed in composites prepared with HNT, indicating that its nanotube structure promotes greater carbon deposition. FTIR and Raman spectrum further confirmed the presence of carbon deposits on the mineral surfaces.

The presence of carbon on the composite surface obtained at 800°C increased the removal efficiency of sulfamethoxazole compared to the raw minerals. The highest removal efficiency was observed for the CHS1a composite (halloysite-based), followed by CHNT1a, and the lowest for CKT1a. The adsorption kinetics of sulfamethoxazole on the most effective adsorbent (CHS1a) followed the pseudo-second-order kinetic model, indicating a chemisorption mechanism. The adsorption process was consistent with the Langmuir adsorption model involving multiple active centers, without dissociation of the sulfamethoxazole molecules.

Halloysite, especially raw halloysite sourced from Polish mines, represents a cost-effective and environmentally friendly carrier that, when combined with carbon, may serve as a suitable adsorbent for sulfamethoxazole in broader applications. The resulting halloysite-carbon composite is an inexpensive, non-flammable, and eco-friendly material due to the use of agricultural waste material as the carbon source.

## Funding

This work was supported by the Ministry of Science, Poland under “Regional Initiative of Excellence” program (research project RID/SP/0015/2024/01).

The publication was financed within the framework of the Ministry of Science and Higher Education research projects SUPB.RN.25.214 and SUPB.RN.25.212.

## Declaration of interest statement:

The authors declare that they have no known competing financial interests or personal relationships that could have appeared to influence the work reported in this paper.

## Data Availability Statement

The authors confirm that the data supporting the findings of this study are available within the article and its supplementary materials.

## References

- Anadao, P., Pajolli, I.L.R., Hildebrando, E.A. & Wiebeck, H. (2014). Preparation and characterization of carbon/montmorillonite composites and nanocomposites from waste bleaching sodium montmorillonite clay, *Advanced Powder Technology* 25, pp. 926–932. DOI.10.1016/j.appt.2014.01.010
- Avisar D., Primor, O., Gozlan, I. & Mamane, H. (2010). Sorption of Sulfonamides and Tetracyclines to Montmorillonite Clay, *Water, Air, & Soil Pollution*, 209, pp.439–450. DOI:10.1007/s11270-009-0212-8
- Bakandritsos, A., Kouvelos, E., Steriotis, T. & Petridis, D. (2005). Aqueous and Gaseous Adsorption from Montmorillonite-Carbon Composites and from Derived Carbons, *Langmuir*, 21, pp. 2349–2355. DOI. 10.1021/la047495g
- Balarak, D., Baniasadi, M., Lee, S.M. & Shim, M.J. (2021). Ciprofloxacin adsorption onto azolla filiculoides activated carbon from aqueous solutions, *Desalination and Water Treatment*, 218, pp. 444–453. DOI.10.5004/dwt.2021.26986
- Bandura, L., Białoszewska, M., Leiviskä, T. & Franus, M. (2022). The role of zeolite structure in its  $\beta$ -cyclodextrin modification and tetracycline adsorption from aqueous solution: characteristics and sorption mechanism, *Materials*, 15, p. 6317. DOI.10.3390/ma15186317
- Bernal, V., Erto, A., Giraldo, L. & Moreno-Piraján, J.C. (2017). Effect of solution pH on the adsorption of paracetamol on chemically modified activated carbons, *Molecules*, 22, p. 1032. DOI.10.3390/molecules22071032
- Biancullo, F., Moreira, N.F.F., Ribeiro, A.R., Manaia, C.M., Faria, J.L., Nunes, O.C., Castro-Silva, S.M. & Silva, A.M.T. (2019). Heterogeneous photocatalysis using UVA-LEDs for the removal of antibiotics and antibiotic resistant bacteria from urban wastewater treatment plant effluents, *Chemical Engineering Journal*, 367, p. 304. DOI.10.1016/j.cej.2019.02.012
- Chen, Y., Li, M., Gao, W., Guan, Y., Hao, Z. & Liu, J. (2024). Occurrence and risks of pharmaceuticals, personal care products, and endocrine-disrupting compounds in Chinese surface waters, *Journal of Environmental Sciences*, 146, pp. 251–263. DOI.10.1016/j.jes.2023.10.011
- Chen, L.-F., Liang, H.-W., Lu, Y., Cui, C.-H. & Yu, S.-H. (2011). Synthesis of an Attapulgite Clay@Carbon Nanocomposite Adsorbent by a Hydrothermal Carbonization Process and Their Application in the Removal of Toxic Metal Ions from Water, *Langmuir*, 27, pp. 8998–9004. DOI.10.1021/la2017165
- Cheng, H., Frost, R.L., Yang, J., Liu, Q. & He, J. (2010). Infrared and infrared emission spectroscopic study of typical Chinese kaolinite and halloysite, *Spectrochimica Acta, Part A*, 77, pp. 1014–1020. DOI.10.1016/j.saa.2010.08.039
- De Oliveira, T., Fernandez, E. L., Fougère, E., Destandau, M., Boussafir, M., Sohmiya, M., Sugahara, Y. & Guégan, R. (2018). Competitive Association of Antibiotics with a Clay Mineral and Organoclay Derivatives as a Control of Their Lifetimes in the Environment, *ACS Omega*, 3, pp. 15332–15342.
- Evers, M., Lange, R.-L., Heinz, E. & Wichern, M. (2022). Simultaneous powdered activated carbon dosage for micropollutant removal on a municipal wastewater treatment plant compared to the efficiency of a post treatment stage, *Journal of Water Process Engineering*, 47, p. 102755. DOI.10.1016/j.jwpe.2022.102755
- Freundlich, H.M.F. (1906). Over the adsorption in solution, *Zeitschrift für Physikalische Chemie*, 57, pp. 385–470.
- Gamoń, F., Tomaszewski, M., Cema, G. & Ziemińska-Buczyńska, A. (2022). Adsorption of oxytetracycline and ciprofloxacin on carbon-based nanomaterials as affected by pH, *Archives of Environmental Protection*, 48, pp. 34–41. doi.org 10.24425/aep.2022.140764
- Gülenay Haciosmanoğlu, G., Mejías, C., Martín, J., Santos, J. L., Aparicio, I. & Alonso, E. (2022). Antibiotic adsorption by natural and modified clay minerals as designer adsorbents for wastewater treatment: A comprehensive review, *Journal of Environmental Management*, 317, p. DOI.115397. 10.1016/j.jenvman.2022.115397
- Ho, Y.S. & McKay, G. (1999). Pseudo-second-order model for sorption processes, *Process Biochemistry*, 34, pp. 451–465. DOI.10.1016/S0032-9592(98)00112-5
- Hu, W., Niu, Y., Dong, K. & Wang, D. (2022). Removal of sulfamethoxazole from aqueous solution onto bagasse derived activated carbon: Response surface methodology, isotherm and kinetics studies, *Journal of Molecular Liquids*, 347, p. 11814. DOI.10.1016/j.molliq.2021.118141



- Jiang, T., Wu, W., Ma, M., Hu, Y. & Li, R. (2024). Occurrence and distribution of emerging contaminants in wastewater treatment plants: A globally review over the past two decades, *Science of The Total Environment*, 951, p. 175664. DOI.10.1016/j.scitotenv.2024.175664
- Jiang, L., Zhang, C., Wei, J., Tjiu, W., Pan, J., Chen, Y. & Liu, T. Surface Modifications of Halloysite Nanotubes with Superparamagnetic Fe<sub>3</sub>O<sub>4</sub> Nanoparticles and Carbonaceous Layers for Efficient Adsorption of Dyes in Water Treatment (2014). *Chemical Research in Chinese Universities*, 30, pp. 971–977. DOI.10.1007/s40242-014-4218-4.
- Joussein, E., Petit, S. & Delvaux, B. (2007). Behavior of halloysite clay under formamide treatment, *Applied Clay Science*, 35, pp. 17–24. DOI.10.1016/j.clay.2006.07.002.
- Kayal, A. & Mandal, S. (2022). Microbial degradation of antibiotic: future possibility of mitigating antibiotic pollution, *Environmental Monitoring and Assessment*, 194, p. 639. DOI.10.1007/s10661-022-10314-2.
- Kodama, S. & Sekiguchi, H. (2006). Estimation of point of zero charge for activated carbon treated with atmospheric pressure nonthermal oxygen plasmas, *Thin Solid Films*, 506–507, pp. 327–330. DOI.10.1016/j.tsf.2005.08.137.
- Lagergren, S. (1898). About the theory of so-called adsorption of soluble substances, *Kungliga Svenska Vetenskapsakademiens, Handlingar*, 24, pp. 1–39.
- Langmuir, I. (1916). The constitutional and fundamental properties of solids and liquids. *Journal of the American Chemical Society*, 38, pp. 2221–2295.
- Leboda, R., Charnas, B., Skubiszewska-Zięba, J. & Chodorowski, S. (2005). Carbon-mineral adsorbents prepared by pyrolysis of waste materials in the presence of tetrachloromethane, *Journal of Colloid and Interface Science*, 284, pp. 39–47. DOI.10.1016/j.jcis.2004.09.052.
- Lim, C.K., Bay, H.H., Neoh, C.H., Aris, A., Majid, Z.A. & Ibrahim, Z. (2013). Application of zeolite-activated carbon macrocomposite for the adsorption of Acid Orange 7: isotherm, kinetic and thermodynamic studies, *Environmental Science and Pollution Research*, 20, pp. 7243–7255. DOI.10.1007/s11356-013-1725-7.
- Liu, Y., Liu, X., Lu, S., Zhao, B., Wang, Z., Xi, B. & Guo, W. (2020). Adsorption and biodegradation of sulfamethoxazole and ofloxacin on zeolite: Influence of particle diameter and redox potential, *Chemical Engineering Journal*, 384, 123346.
- Lu, Z.-Y., Ma, Y. L., Zhang, J.-T., Fan, N.-S., Huang, B.-Ch. & Jin, R.-C. (2020). A critical review of antibiotic removal strategies: Performance and mechanisms, *Journal of Water Process Engineering*, 38, p. 101681. DOI.10.1016/j.jwpe.2020.101681.
- Luo, J., Li, X., Ge, C., Müller, K., Yu, H., Huang, P., Li, J., Tsang, D.C.W., Bolan, N.S., Rinklebe, J. & Wang, H. (2018). Sorption of norfloxacin, sulfamerazine and oxytetracycline by KOH modified biochar under single and ternary systems, *Bioresource Technology*, 263, pp. 385–392. DOI.10.1016/j.biortech.2018.05.022.
- Ma, Y., Yang, L., Wu, L., Li, P., Qi, X., He, L., Cui, S., Ding, Y. & Zhang, Z. (2020). Carbon nanotube supported sludge biochar as an efficient adsorbent for low concentrations of sulfamethoxazole removal, *Science of The Total Environment*, 718, p. 137299. DOI.10.1016/j.scitotenv.2020.137299
- Parida, V. K., Saidulu, D., Majumder, A., Srivastava, A., Gupta, B. & Gupta, A. K. (2021). Emerging contaminants in wastewater: A critical review on occurrence, existing legislations, risk assessment, and sustainable treatment alternatives, *Journal of Environmental Chemical Engineering*, 9, p. 105966. DOI.10.1016/j.jece.2021.105966.
- Prasannamedha, G. & Senthil, K.P. (2019). A review on Contamination and Removal of Sulfamethoxazole from Aqueous Solution using Cleaner Techniques: Present and Future Perspective, *Journal of Cleaner Production*, 250(5), p. 119553. DOI.10.1016/j.jclepro.2019.119553.
- Qalyoubi, L., Al-Othman, A., Al-Asheh, S., Shirvanimoghaddam, K., Mahmoodi, R. & Naebe, M. (2024). Textile-based biochar for the removal of ciprofloxacin antibiotics from water, *Emergent Materials*, 7, pp. 577–588. DOI.10.1007/s42247-023-00512-0.
- Sagaseta de Ilurdoz, M., Jaime Sadhwani, J. & Vaswani Reboso, J. (2022). Antibiotic removal processes from water & wastewater for the protection of the aquatic environment – a review, *Journal of Water Process Engineering*, 45, p. 102474. DOI.10.1016/j.jwpe.2021.102474.
- Sing, K.S.W., Everett, D.H., Haul, R.A.W., Moscou, L., Pierotti, R.A., Rouquerol, J. & Siemieniowska, T. (1985). Reporting physisorption data for gas/solid systems with special reference to the determination of surface area and porosity, *Pure and Applied Chemistry*, 57, pp. 603–619. DOI.10.1351/pac198254112201.
- Skubiszewska-Zięba, J., Charnas, B., Leboda, R. & Gun'ko, V.M. (2012). Carbon-mineral adsorbents with a diatomaceous earth/perlite matrix modified by carbon deposits, *Microporous and Mesoporous Materials*, 156, pp. 209–216. DOI.10.1016/j.micromeso.2012.02.038.
- Szczepanik, B., Banaś, D., Kubala-Kukuś, A., Szary, K., Słomkiewicz, P., Rędzia, N. & Frydel, L. (2020). Surface Properties of Halloysite-Carbon Nanocomposites and Their Application for Adsorption of Paracetamol, *Materials*, 13, p. 5647. DOI.10.3390/ma13245647.
- Szczepanik, B., Frydel, L., Słomkiewicz, P. M., Banaś, D., Stabrawa, I. & Kubala-Kukuś, A. (2023). Adsorptive removal of chloroxylenol and chlorophene from aqueous solutions using carbon-halloysite nanocomposites obtained from corrugated cardboard as a carbon precursor, *Desalination and Water Treatment*, 288, pp. 93–103. DOI.10.5004/dwt.2023.29212.
- Szczepanik, B., Rędzia, N., Frydel, L., Słomkiewicz, P., Kołbus, A., Stysko, K. & Samojeden, B. (2019). Synthesis and Characterization of Halloysite/Carbon Nanocomposites for Enhanced NSAIDs Adsorption from Water, *Materials*, 12, p. 3754. DOI.10.3390/ma12223754.
- Tan, X., Wei, H., Zhou, Y., Zhang, Ch. & Ho, S.-H. (2022). Adsorption of sulfamethoxazole via biochar: The key role of characteristic components derived from different growth stage of microalgae, *Environmental Research*, 210, p. 112965. DOI.10.1016/j.envres.2022.112965.
- Tang, L., Yu, J., Pang, Y., Zeng, G., Deng Y., Wang, J., Ren, X., Ye, S., Peng B. & Feng, H. (2018). Sustainable efficient adsorbent: alkali-acid modified magnetic biochar derived from sewage sludge for aqueous organic contaminant removal, *Chemical Engineering Journal*, 336, pp. 160–169. DOI.10.1016/j.cej.2017.11.048.
- Temkin, M.I. & Pyzhev, V. (1940). Kinetics of ammonia synthesis on promoted iron catalyst, *Acta USSR* 12, 3, pp. 27–356.
- Terzyk, A. P. (2001). The influence of activated carbon surface chemical composition on the adsorption of acetaminophen (paracetamol) in vitro: Part II. TG, FTIR, and XPS analysis of

- carbons and the temperature dependence of adsorption kinetics at the neutral pH, *Colloids and Surfaces*, 177, pp. 23–45. DOI:10.1016/S0927-7757(00)00594-X.
- Wang, J. & Zhuan, R. (2020). Degradation of antibiotics by advanced oxidation processes: An overview, *Total Environment*, 701, p. 135023. DOI:10.1016/j.scitotenv.2019.135023.
- Weber, W.J. & Morris, J.C. (1963). Kinetics of adsorption on carbon solution, *Journal of the Sanitary Engineering Division Am. Soc. Civ. Eng.*, 89, pp. 31–59.
- Wu, X., Gao, P., Zhang, X., Jin, G., Xu, Y. & Wu, Y. (2014). Synthesis of clay/carbon adsorbent through hydrothermal carbonization of cellulose on palygorskite, *Applied Clay Science*, 95, pp. 60–66. DOI:10.1016/j.clay.2014.03.010.
- Wu, X., Liu, C., Qi, H., Zhang, X., Dai, J., Zhang, Q., Zhang, L., Wu, Y. & Peng, X. (2016). Synthesis and adsorption properties of halloysite/carbon nanocomposites and halloysite-derived carbon nanotubes, *Applied Clay Science*, 119, pp. 284–293. DOI:10.1016/j.clay.2015.10.029.
- Wu, X., Xu, Y., Zhang, X., Wu, Y. & Gao, P. (2015). Adsorption of low-concentration methylene blue onto a palygorskite/carbon composite, *New Carbon Materials*, 30, pp. 71–78. DOI:10.1016/S1872-5805(24)60878-4.
- Wu, X., Zhu, W., Zhang, X., Chen, T. & Frost, R.L. (2011). Catalytic deposition of nanocarbon onto palygorskite and its adsorption of phenol, *Applied Clay Science*, 52, pp. 400–406. DOI:10.1016/j.clay.2011.04.011.
- Xiang, Y., Xu, Z., Wei, Y., Zhou, Y., Yang, X., Yang, Y., Yang, J., Zhang, J., Luo, L. & Zhou, Z. (2019). Carbon-based materials as adsorbent for antibiotics removal: Mechanisms and influencing factors, *Journal of Environmental Management*, 237, pp. 128–138. DOI:10.1016/j.jenvman.2019.02.068.
- Yuan, P., Tan, D., Annabi-Bergaya, F., Yan, W., Fan, M., Liu, D. & He, H. (2012). Changes in structure, morphology, porosity, and surface activity of mesoporous halloysite nanotubes under heating, *Clays and Clay Minerals*, 60(6), pp. 561–573. DOI:10.1346/CCMN.2012.0600602.
- Zhang, Ch., Wang, L., Gao, X. & He, X. (2016). Antibiotics in WWTP discharge into the Chaobai River, Beijing, *Archives of Environmental Protection*, 42, pp. 48–57. DOI:10.1515/aep-2016-0036.
- Zhao, J., Han, Y., Liu, J., Li, B., Li, J., Li, W., Shi, P., Pan, Y., & Li, A. (2024). Occurrence, distribution and potential environmental risks of pollutants in aquaculture ponds during pond cleaning in Taihu Lake Basin, China, *Science of The Total Environment*, 939, p. 173610. DOI: 10.1016/j.scitotenv.2024.173610.
- Zhao, J. (2023). Molecular imprinting functionalization of magnetic biochar to adsorb sulfamethoxazole: Mechanism, regeneration and targeted adsorption, *Process Safety and Environmental Protection*, 171, pp. 238–249. DOI:10.1016/j.psep.2023.01.024.
- Zhao, T., Ali, A., Su, J., Liu, S., Yan, H. & Xu, L. (2024). Removal of sulfamethoxazole from water by biosurfactant-modified sludge biochar: Properties and mechanism, *Journal of Environmental Chemical Engineering*, 12, p.114200. DOI:10.1016/j.jece.2024.114200.
- Zhao, Z. & Zhou, W. (2019). Insight into interaction between biochar and soil minerals in changing biochar properties and adsorption capacities for sulfamethoxazole, *Environmental Pollution*, 245, pp. 208–217. DOI: 10.1016/j.envpol.2018.11.013

## Adsorpcyjne usuwanie sulfametoksazolu z wody na kompozytach węglowo-mineralnych

**Streszczenie.** Celem tej pracy była synteza nowych kompozytów węglowo-mineralnych i ich wykorzystanie do usuwania sulfametoksazolu z wody. Kompozyty węglowo-haloizytowe (CHS1a,b, CHNT1a,b) i węglowo-kaolinitowe (CKT1a,b) otrzymano z odpadowych wytlóków owocowych jako prekursora węgla. Ponadto surowy haloizyt (HS), nanorurki haloizytowe (HNT) i kaolinit (KT) wykorzystano jako nośniki w procesie karbonizacji w atmosferze N<sub>2</sub> dla dwóch temperatur: 500oC i 800oC. Morfologię i charakterystykę strukturalną otrzymanych kompozytów zbadano przy użyciu metod SEM EDX, FT-IR i spektroskopii Ramana oraz metod adsorpcji azotu w niskiej temperaturze. Wszystkie kompozyty były materiałami mezoporowatymi. Wyniki SEM i FTIR potwierdziły, że powierzchnia HNT, HS i KT jest pokryta węglem. Najwyższa zawartość węgla w kompozytach z HNT wskazuje, że struktura nanorurek wpływa na osadzanie węgla na ich powierzchni. Badano również adsorpcję sulfametoksazolu na nowych kompozytach węglowo-mineralnych i minerałach niemodyfikowanych. Efektywność usuwania sulfametoksazolu znacznie wzrosła w przypadku takich kompozytów jak: CHS1a, CHNT1a i CKT1a otrzymanych w temperaturze 800oC w porównaniu do minerałów surowych. Optymalne warunki usuwania sulfametoksazolu, umożliwiające najwyższą efektywność usuwania 84%, obejmują zastosowanie masy adsorbentu CHS1a wynoszącej 6 g/dm<sup>3</sup> przy początkowym stężeniu roztworu antybiotyku 20 mg/dm<sup>3</sup>. Proces adsorpcji sulfametoksazolu na najlepszym adsorbencie CHS1a opisuje model kinetyczny pseudo-drugiego rzędu i wielocentrowy model adsorpcji Langmuira. Kompozyt CHS1a można stosować jako potencjalny adsorbent do usuwania sulfametoksazolu z wody.